LARGE-SCALE PATTERNS ON THE SUN OBSERVED IN THE MILLIMETRIC WAVELENGTH RANGE

B. VRŠNAK[1], S. POHJOLAINEN[2], S. URPO[2], H. TERÄSRANTA[2], R. BRAJŠA[1], V. RUŽDJAK[1], Z. MOURADIAN[3], and S. JURAČ[4]

(Received 16 April, 1991; in revised form 23 July, 1991)

Abstract. The nature and behaviour of large-scale patterns on the solar surface, indicated by the areas of brightness-temperature depressions in the millimetric wavelength range, is studied. A large sample of 346 individual, low-temperature regions (LTRs) was employed to provide reliable statistical evidence. An association of 99% was found between the locations of LTRs and the large-scale magnetic field inversion lines, and 60% of the LTRs were associated with the inversion line filaments. A tentative physical association with filaments is reconsidered, and one particularly well-observed case is presented. The heights of the perturbers causing brightness-temperature depressions are discussed. The long-term evolution of the latitudinal distribution of LTRs is presented in a butterfly diagram. Two belts of low-temperature regions outline the active region belts, shifting with them towards the equator during the solar activity cycle. The low-temperature region belts of the forthcoming cycle appear already at the maximum of the actual cycle at latitudes of about 55°. The superpositions of the temperature minima distributions in the synoptic maps show patterns appearing as 'giant cells' and compatible with indications inferred from magnetographic data. The reliability of the inferred cells is considered, and a statistical analysis reveals a negligible probability for an accidental distribution appearing in the form of giant cells.

1. Introduction

Observations of the Sun in the millimetric wavelength range reveal three categories of stable features. The most prominent ones are large-amplitude enhancements of the brightness temperature associated with active regions. The second type of features appearing within the latitude belt $\pm 55°$, are the areas of low-amplitude brightness temperature depressions (Hiei *et al.*, 1986, and references therein), which can be detected only in high-sensitivity contour maps. The third type of features are areas of low-amplitude brightness temperature enhancements which may be found in polar regions (Urpo *et al.*, 1989). We call a temperature depression area a 'Low Temperature Region' (LTR) and a temperature enhancement area a 'High Temperature Region' (HTR). In this paper we shall study especially the LTRs.

The most extensive studies on the nature of LTRs were performed by Schmahl, Bobrowsky, and Kundu (1981) and Hiei *et al.* (1986) who related the LTRs with quiescent filaments and the magnetic inversion lines. Some observations of LTRs were used to determine the solar differential rotation (Liu and Kundu, 1976; Urpo *et al.*, 1989; Pohjolainen *et al.*, 1991) and LTRs seem to be useful tracers to determine the

[1] Hvar Observatory, Faculty of Geodesy, Kačićeva 26, 41000 Zagreb, Croatia, Yugoslavia.
[2] Metsähovi Radio Research Station, 02540 Kylmala, Finland.
[3] Observatoire de Paris, DASOP, 92195 Meudon, France.
[4] Astronomical Observatory Zagreb, Opatička 22, 41000 Zagreb, Croatia, Yugoslavia.

Solar Physics **137:** 67–86, 1992.

rotation rate of large scale patterns on the solar surface. However, the previous studies were based on small samples and were limited by short observational intervals.

2. The Data Set

We present a study based on a large sample of data, covering a long time period. Processing of solar maps started at the Metsähovi Radio Research Station (Finland) in 1978, based on the observations obtained by the 13.7 m diameter dish radio-telescope (Urpo, Pohjolainen, and Teräsranta, 1987). In TablesIa–II microwave observations performed in the years 1979, 1980, 1981, 1982, 1987, 1988, and 1989 and used in this study are presented. The dates, the number of 37 GHz maps per day (N) and the number of identified temperature minima (N_{LTR}) are presented.

The observations were performed from 2 up to 10 weeks per year and were carried out at the frequencies of 12 GHz (26 mm), 22 GHz (13 mm), 37 GHz (8 mm), and 87 GHz (4 mm). Often, several maps per day were obtained. Most of the solar maps were obtained by scanning the Sun in right ascension at 37 GHz. In the following analysis we consider only the maps of the solar disc observed at 37 GHz, where the

TABLE Ia

List of microwave observations in the period May/June 1979

Date	N	N_{LTR}	Date	N	N_{LTR}
6 May, 1979	1	3	29 May, 1979	1	7
8 May, 1979	2	3	30 May, 1979	1	7
13 May, 1979	1	4	31 May, 1979	1	4
14 May, 1979	1	4	1 June, 1979	1	7
15 May, 1979	1	4	2 June, 1979	1	5
18 May, 1979	1	4	3 June, 1979	1	2
19 May, 1979	1	5	4 June, 1979	1	4
20 May, 1979	1	5	5 June, 1979	1	4
21 May, 1979	1	6	6 June, 1979	2	5
22 May, 1979	1	4	7 June, 1979	2	5
25 May, 1979	1	5	8 June, 1979	1	4
26 May, 1979	1	7	10 June, 1979	2	4
27 May, 1979	1	6	11 June, 1979	1	1
28 May, 1979	1	4	12 June, 1979	1	1

TABLE Ib

List of microwave observations in the period October 1979

Date	N	N_{LTR}	Date	N	N_{LTR}
5 Oct., 1979	2	2	7 Oct., 1979	2	4
6 Oct., 1979	2	4	9 Oct., 1979	1	1

TABLE Ic

List of microwave observations in the period May/June 1980

Date	N	N_{LTR}	Date	N	N_{LTR}
29 May, 1980	1	4	9 June, 1980	1	3
30 May, 1980	1	4	10 June, 1980	1	5
2 June, 1980	1	6	11 June, 1980	1	3
3 June, 1980	1	5	12 June, 1980	1	1
4 June, 1980	1	4	13 June, 1980	1	6
5 June, 1980	2	6	14 June, 1980	1	5
6 June, 1980	1	5	15 June, 1980	1	8
7 June, 1980	1	4	16 June, 1980	1	9
8 June, 1980	1	3	17 June, 1980	1	6

TABLE Id

List of microwave observations in the period September/October 1980

Date	N	N_{LTR}	Date	N	N_{LTR}
9 Sept., 1980	1	1	24 Sept., 1980	2	6
10 Sept., 1980	1	7	25 Sept., 1980	2	7
11 Sept., 1980	1	8	26 Sept., 1980	1	7
12 Sept., 1980	1	9	27 Sept., 1980	2	7
13 Sept., 1980	1	6	28 Sept., 1980	1	3
17 Sept., 1980	1	6	29 Sept., 1980	1	2
18 Sept., 1980	1	4	30 Sept., 1980	1	3
19 Sept., 1980	1	7	1 Oct., 1980	1	3
22 Sept., 1980	1	7	3 Oct., 1980	1	2

TABLE Ie

List of microwave observations in the period May/June 1981

Date	N	N_{LTR}	Date	N	N_{LTR}
4 May, 1981	1	3	23 May, 1981	1	9
5 May, 1981	1	6	24 May, 1981	1	5
6 May, 1981	1	9	1 June, 1981	1	4
7 May, 1981	1	9	2 June, 1981	1	8
8 May, 1981	1	7	3 June, 1981	1	6
10 May, 1981	1	6	4 June, 1981	1	4
11 May, 1981	1	12	5 June, 1981	1	5
12 May, 1981	1	13	6 June, 1981	1	4
13 May, 1981	1	13	8 June, 1981	1	8
14 May, 1981	1	10	9 June, 1981	1	8
16 May, 1981	1	11	12 June, 1981	1	7
17 May, 1981	1	13	15 June, 1981	1	4
18 May, 1981	1	10	18 June, 1981	1	1
19 May, 1981	1	8	28 June, 1981	1	4
20 May, 1981	1	7	29 June, 1981	1	6
21 May, 1981	1	7	30 June, 1981	1	6
22 May, 1981	1	7			

TABLE If

List of microwave observations in the period September/October 1981

Date	N	N_{LTR}	Date	N	N_{LTR}
17 Sept., 1981	1	3	27 Sept., 1981	1	4
18 Sept., 1981	1	3	28 Sept., 1981	1	7
19 Sept., 1981	1	3	29 Sept., 1981	1	8
20 Sept., 1981	1	4	30 Sept., 1981	1	5
21 Sept., 1981	1	1	1 Oct., 1981	1	7
24 Sept., 1981	1	2	2 Oct., 1981	1	8
25 Sept., 1981	1	2	3 Oct., 1981	1	8

TABLE Ig

List of microwave observations in the period July 1982

Date	N	N_{LTR}	Date	N	N_{LTR}
15 July, 1982	1	6	17 July, 1982	1	6
16 July, 1982	1	6	18 July, 1982	1	6

TABLE Ih

List of microwave observations in the period May 1987

Date	N	N_{LTR}	Date	N	N_{LTR}
15 May, 1987	1	6	24 May, 1987	1	6
16 May, 1987	1	10	25 May, 1987	2	9
17 May, 1987	1	7	26 May, 1987	1	10
19 May, 1987	1	10	27 May, 1987	1	4
20 May, 1987	1	6	28 May, 1987	1	5
21 May, 1987	1	7	29 May, 1987	2	7
22 May, 1987	1	7	30 May, 1987	1	6
23 May, 1987	1	4	31 May, 1987	1	5

TABLE Ii

List of microwave observations in the period August/September 1987

Date	N	N_{LTR}	Date	N	N_{LTR}
17 Aug., 1987	1	2	27 Aug., 1987	1	8
20 Aug., 1987	1	7	31 Aug., 1987	1	9
22 Aug., 1987	1	9	2 Sept., 1987	1	8
24 Aug., 1987	1	11	3 Sept., 1987	1	8
25 Aug., 1987	1	10	4 Sept., 1987	1	4
26 Aug., 1987	1	10	6 Sept., 1987	1	5

TABLE Ij

List of microwave observations in the period April/May 1988

Date	N	N_{LTR}	Date	N	N_{LTR}
12 Apr., 1988	3	5	9 May, 1988	2	5
13 Apr., 1988	1	5	10 May, 1988	1	6
15 Apr., 1988	1	5	11 May, 1988	1	6
4 May, 1988	1	3	12 May, 1988	1	7
5 May, 1988	1	3	13 May, 1988	1	6
6 May, 1988	1	3	14 May, 1988	1	3
7 May, 1988	1	2	15 May, 1988	1	3
8 May, 1988	4	5			

TABLE Ik

List of microwave observations in the period September 1988

Date	N	N_{LTR}	Date	N	N_{LTR}
6 Sept., 1988	3	8	11 Sept., 1988	1	2
9 Sept., 1988	3	3			

TABLE Il

List of microwave observations in the period June 1989

Date	N	N_{LTR}	Date	N	N_{LTR}
20 June, 1989	4	9	25 June, 1989	2	4
21 June, 1989	3	7	26 June, 1989	2	5
22 June, 1989	3	7	27 June, 1989	3	6
23 June, 1989	2	3	28 June, 1989	2	4
24 June, 1989	1	4	30 June, 1989	1	2

number of data points varied from one thousand to several thousand. The telescope beam size at 37 GHz is 2.4 arc min. In the temperature scale, the resolution is always better than 1% of the quiet Sun level, which is estimated to have a brightness temperature of 7800 K in all maps. A computer program provides coordinates on the solar disc with an accuracy of one heliographic degree at the disc center.

Typical observed dimensions of the LTRs were between several arc minutes and 10 arc min, but one must take into account beam/convolution effects which apparently increase the size of small sources. Durations of the LTRs were between 3 and 7 days but the real lifetime is probably longer since the visibility of LTRs is significantly reduced close to the limb. The usual temperature depression measured at 37 GHz was several hundred K, but sometimes it was as large as 1000 K (again the beam/convolution effect tends to decrease the amplitude of temperature perturbation of small sources). In Figure 1, as an example, we present the synoptic map of the inferred magnetic field

inversion lines (McIntosh, 1972) and contours of LTRs clearly tracing them. As the contours of LTRs depend on the choice of the isothermal-line level (and of course on the ratio of the source size and the telescope beam size), we based our analysis on the

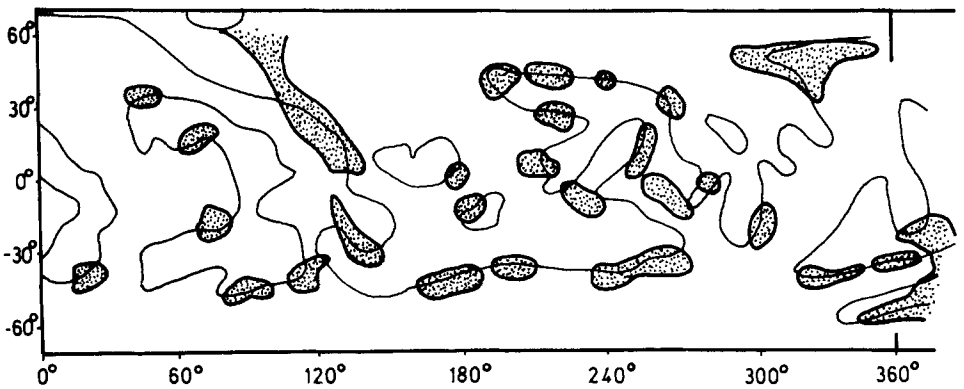

Fig. 1. Synoptic map of Carrington rotation No. 1708. Thin lines represent the inversion lines of the inferred magnetic fields (*Soln. Dann. Bull.*) and the shaded areas show the shapes of the LTRs.

temperature minima positions within LTRs. By LTR we denote further on a group of such positions observed during one Carrington rotation within a particular temperature depression (Figure 2). Our sample consisted of 346 individual LTRs based on more than one thousand positions of temperature minima.

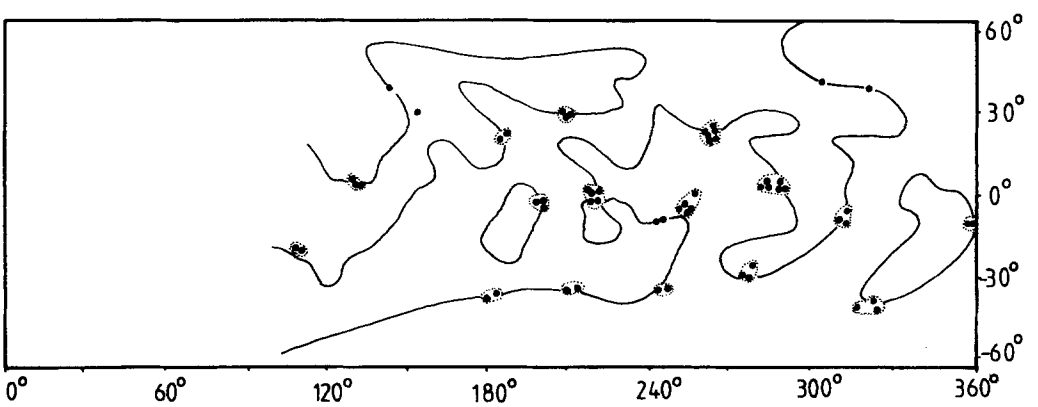

Fig. 2. Synoptic map of Carrington rotation No. 1709. Thin lines represent the inversion lines of the inferred magnetic fields (SGD) and the dots show the positions of the brightness temperature minima within LTRs (outlined by dotted lines).

The positions and orientations of filaments were provided by Meudon patrol Hα-observations. We considered the actual Carrington rotation, as well as the preceding and the following one. The synoptic maps presenting the inferred magnetic fields were

taken from *Solar Geophysical Data* (SGD) and *Solnechnye Dannye Byulleten* (SDB). Finally we used the magnetographic observations presented by Bumba (1987) to compare the inferred large-scale cells (Section 6).

3. Distribution of LTRs across the Solar Disc

We present the central meridian distance (CMD) distribution of LTR positions across the solar disc in Figure 3(a), to show the visibility function. The distributions presented separately for the periods 1979–1982 (sample of 730 temperature minima) and 1987–1989 (351 temperature minima) are also indicated to illustrate the magnitudes of the statistical fluctuations. The visibility function has a maximum between 10° and 20° of CMD, and only few LTRs are found at CMD > 55°.

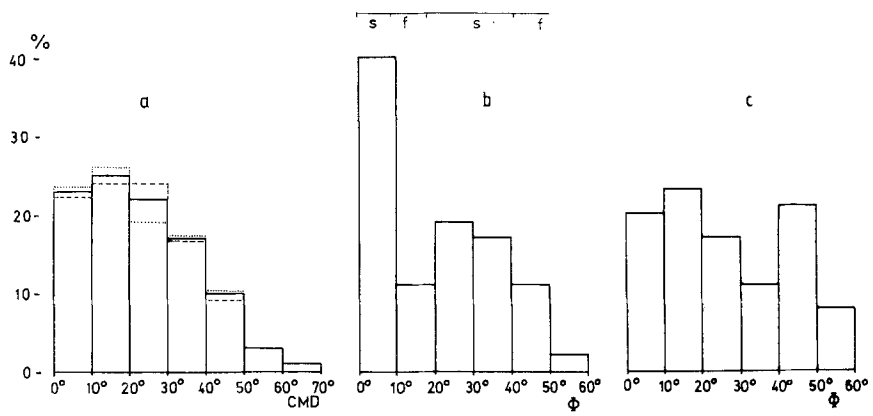

Fig. 3. (a) Visibility of LTRs as a function of CMD; the full line represents the whole sample, the dashed line the 1979–1982 sample and the dotted line the 1987–1989 sample. (b) Latitudinal distribution of LTRs in the period 1979–1982. The belts of slow and fast rotation, as presented by Howard and LaBonte (1980) are denoted by the letters *s* and *f*, respectively. (c) Latitudinal distribution of LTRs in the period 1987–1989.

The latitudinal distribution in ten degree intervals is presented in Figures 3(b) and 3(c) independently for the periods 1979–1982 (maximum and descent of solar activity) and 1987–1989 (minimum and ascension of solar activity). The distributions are significantly different from the CMD distribution, revealing two maxima in each sample. The positions of the maxima changed in the course of the solar cycle. In the period embracing the maximum of solar cycle 21 one finds the minimum in the latitudinal distribution in the belt of latitudes 10°–30°, corresponding to the active region belt in this phase of the cycle. In the period preceding the maximum of cycle 22 (1987–1989) one finds two minima: one embracing the equator and another one in the latitude belt 30°–40°, corresponding to the active region belts of cycles 21 and 22, respectively. Such a behaviour reveals an evolution of the latitudinal distribution during the cycle.

In Figure 4 we present a sketch of the LTR butterfly diagram obtained by inspecting maxima and minima in LTR latitudinal distributions in all of the observational intervals. The LTR belts border the active region belt, shifting simultaneously with active regions towards the equator as the activity of the solar cycle declines. During the activity maximum of the actual cycle, at latitudes higher than 50°, one finds a new LTR belt being a part of a cradle for the forthcoming cycle. It also shifts towards the equator and later on (1987–1989) borders the active regions of the new cycle (Figure 3(c)).

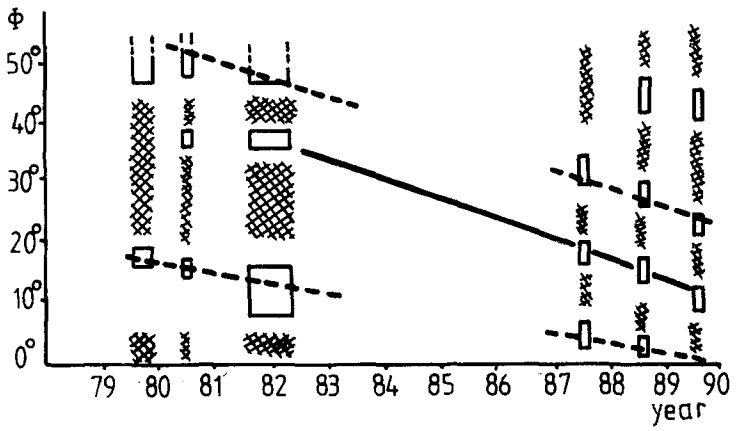

Fig. 4. Latitudinal distribution of LTRs schematically presented in the Butterfly diagram. Hatched areas and unshaded rectangles represent maxima and minima in the distribution, respectively. Dashed lines represent the active region belts of the actual and the forthcoming cycle. The bold lines illustrate the 'border' between the cycles.

The polar crown, defined by a line of prominences oriented nearly parallel to the equator and outlining the polar caps (Tandberg-Hanssen, 1977) could also be detected on the microwave maps as a belt-like zone of LTRs. However, in our observations LTRs were not clearly identified at latitudes higher than 55° and we could not establish reliably a poleward migration of this belt (Tandberg-Hanssen, 1977). This Polar Crown belt of LTRs separates HTRs in polar regions from the large-amplitude HTRs in the sunspot zone and LTRs corresponding to the Royal Zone prominences (the prominences migrating in the butterfly diagram equatorward together with sunspots). The broken lines in Figure 4 depict the active region belts of cycles 21 and 22, and the bold line illustrates a 'border' between the cycles. Let us stress that the precursor of the new solar cycle appears in the LTR distribution already during the maximum of the preceding 11-year cycle, i.e., much earlier than the active regions themselves.

4. Association of LTRs with Magnetic Inversion Lines

The positions and shapes of LTRs superposed onto the inversion lines of the global magnetic fields drawn in Figure 1 show that the regions of decreased brightness tem-

perature trace these lines. We applied two procedures to establish the association rate between LTRs and the inversion lines. The first considers the positions of the centers of LTRs (defined as a group of temperature minima – a sample consisting of 346 LTRs). The second is based on the positions of all temperature minima measured (a sample consisting of 1081 positions). We considered an association as positive if the distance of a LTR (or temperature minimum) from the nearest inversion line was less than the telescope resolution. Both procedures give the same statistical results.

When the locations of LTRs are superposed onto the SGD, maps of the inferred photospheric magnetic fields, one finds that more than 90% of LTRs were situated on the inversion lines. This is a very high association rate, as the method of the inferred large-scale fields cannot always provide reliable results, and in dubious situations it is liable to subjective impressions (McIntosh, 1972). Therefore, we superposed the LTR positions also onto the SDB inversion lines and we found again, a 90% association rate, but now almost all LTRs which were apart from the SGD inversion lines coincided with the SDB inversion lines. Only about 1% of LTRs were not related to either SGD or SDB inversion lines, revealing an extremely high correlation. To illustrate the association, in Figure 2 we present the LTRs positions during the Carrington rotation No. 1709. It is worth noting that a large fraction of LTRs was situated at positions where the inversion lines were sharply curved or at the locations appearing as tongues or throats in the large-scale magnetic fields patterns.

5. Association of LTRs and Filaments

Schmahl, Bobrowsky, and Kundu (1981) and Hiei *et al.* (1986) reported observations of rather small samples of LTRs and concluded that LTRs are most probably caused by absorption in cold and dense prominence plasma (Chiuderi-Drago, 1990). An additional support to this interpretation were the measurements of rotation rates of the LTRs: a rather small sample of 22 LTRs, observed at 35 GHz from March 6 to March 30, 1972 was studied by Liu and Kundu (1976). The LTR tracers used were on average rotating faster than the solar surface corresponding to an average height of 35 000 km for the LTR perturbers, which is a typical height of quiescent solar prominences.

Since quiescent filaments are aligned along the inversion lines of the large-scale magnetic fields and occupy a considerable part of those, an association of LTRs and filaments can be accidental, especially when small samples are considered, as in the studies mentioned. If a larger sample is used to compare the positions of filaments and the positions of LTRs, one finds typically a 60–70% association (applying the same criteria as for the magnetic inversion lines) on different synoptic maps. However, taking into account the filaments in the preceding and following rotations one finds a higher association rate: only 10% of LTRs in our sample were without an associated filament as illustrated by Figure 5 (the indicated dimension of an LTR is defined by the dispersion of temperature minima positions. We want to stress that there is a large number of filaments which do not produce any observable temperature depression, and since a

rather high fraction of LTRs was not associated with filaments directly, the association can be statistically accidental. Finally let us point out that we could not find any statistical correlation between the filament geometry (length, height, and width) and the area or the amplitude of the LTR.

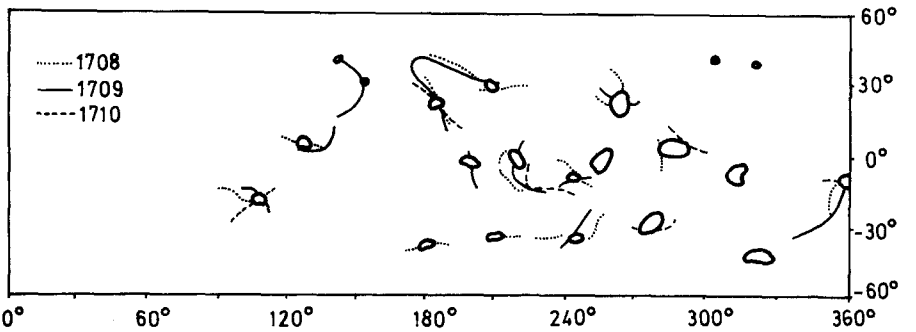

Fig. 5. Synoptic map of Carrington rotation No. 1709. The oval shapes represent LTRs and the lines represent the positions of associated filaments in the preceding rotation (1708) and the following rotation (1710).

The relation between filaments and LTRs can be studied directly by simultaneous observations in the Hα line and microwaves. As an illustration we present the observations of the most prominent LTR in our sample (Figures 6(a) and 6(b)) and the associated filament (Figures 6(c) and 6(d)) during their disc passage in July 1982. The LTR was visible at 37 GHz, as well as at 22 GHz during several days (Table II). The SGD and SDB Hα-reports show a huge quiescent filament associated with the LTR. The filament was aligned roughly in the north–south direction, obviously not belonging to the Polar Crown (Tandberg-Hanssen, 1977). It extended from the latitude $\phi_f = 25°$ to $\phi_f = 70°$ in the northern hemisphere and was located at a longitude of about $\lambda_f = 300°$. The associated LTR was detectable at a latitude of $\phi_{\mathrm{LTR}} = 50°–55°$ and at the same longitude as the filament. The positions of the LTR observed at 22 and 37 GHz at the time of measurements (UT) are presented in Table II, where the indices represent the radio frequency. The CMDs of the filament body (CMD_f) measured at the LTR latitude and the CMDs of the closest footpoints (CMD_{fp}) are presented in Table III. Although the LTR and the filament were at the same longitude within the accuracy of measurements, the estimated positions of 37 GHz temperature minima (corrected for the time difference between the Hα and microwave observations) were always at the edges of the filament closer to the central meridian, indicating a lower height of the LTR.

The apparent synodic rotation rates of the LTR obtained by tracing the position of the temperature minima at 22 and 37 GHz were 14.7 ± 0.9 and 13.5 ± 0.4 deg day^{-1}, respectively. The part of the filament body at the same latitude showed an apparent synodic rotation (14.6 ± 0.4 deg day^{-1}) implying that the 37 GHz LTR perturber was lower than the main prominence body while the 22 GHz perturber was at about the same height as the prominence body. The synodic rotation rate of the filament footpoints was

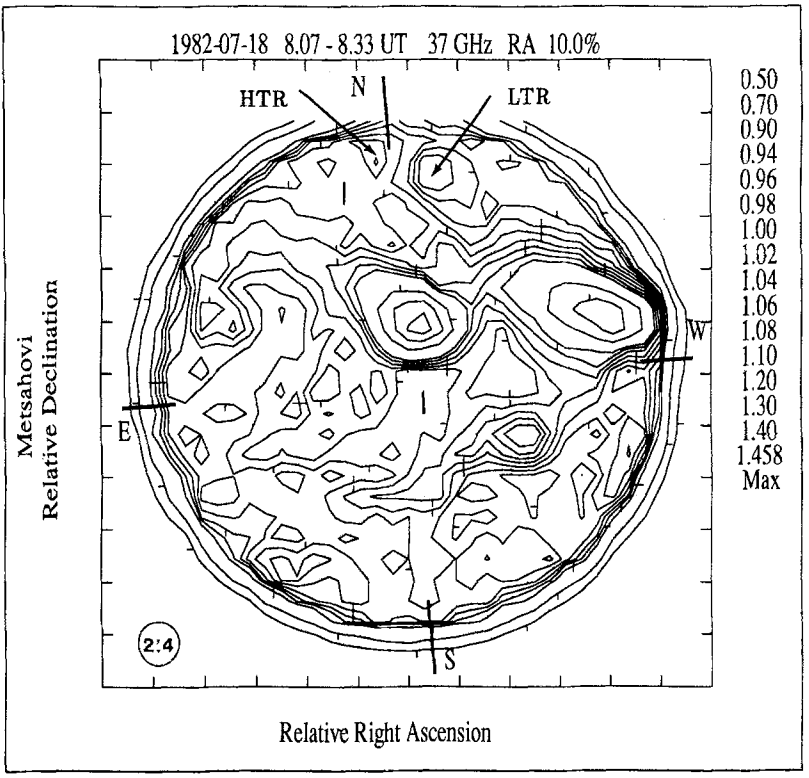

Fig. 6a.

Fig. 6. Disc passage of the 'July '82 LTR' (denoted as LTR). The maps presented were obtained on July (16) (a) and July 18 (b). The temperature minimum studied indicated together with an active region (AR) a weak brightness temperature enhancement close to the pole (HTR). The direction of the temperature gradient is depicted by the mark normal to the isothermal lines, pointing towards lower temperatures. The numbers on the right-hand side are the contour levels with respect to the quiet-Sun level (7800 K). Disc passage of the filament associated with the 'July '82 LTR' is presented in (c) and (d).

10.8 ± 1.8 deg day^{-1}, which is an appropriate value for surface rotation at these latitudes.

The temperature depressions at 37 GHz (ΔT_{37}) and 22 GHz (ΔT_{22}) are given in Table II. During July 15, 16, and 17, the temperature depression at 37 GHz was about 11% of the quiet Sun level, and on July 18 it was reduced to 6%. This 'temperature increase' is probably associated with the disappearance of the Hα filament on July 19, i.e., it could be a consequence of changing coronal conditions above the inversion line, but other reasons cannot be excluded. A similar behaviour, but with flatter depressions, was also found at 22 GHz (Table II). Unfortunately we have no microwave measurements after July 18.

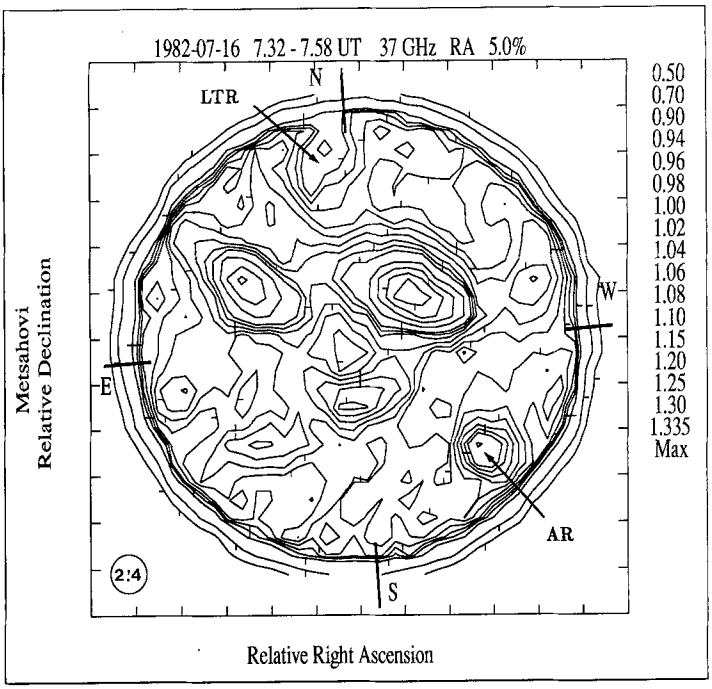
1982-07-16 7.32 - 7.58 UT 37 GHz RA 5.0%
N
LTR
W
E
S
AR
2:4
0.50
0.70
0.90
0.94
0.96
0.98
1.00
1.02
1.04
1.06
1.08
1.10
1.15
1.20
1.25
1.30
1.335
Max
Metsahovi
Relative Declination
Relative Right Ascension

Fig. 6b.

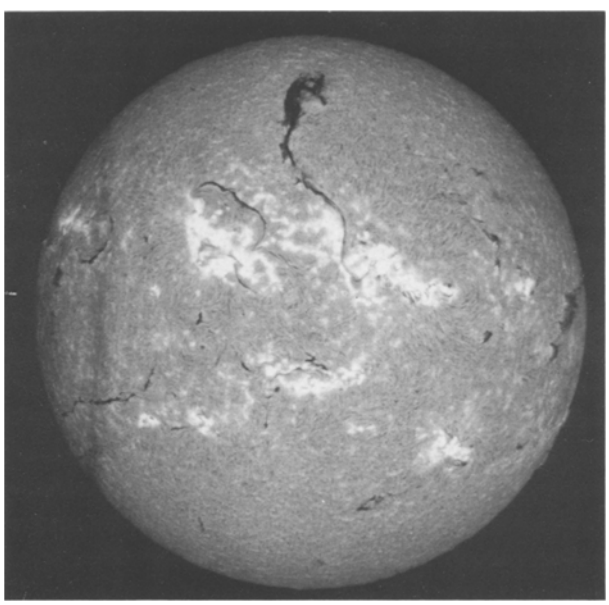

Fig. 6c.

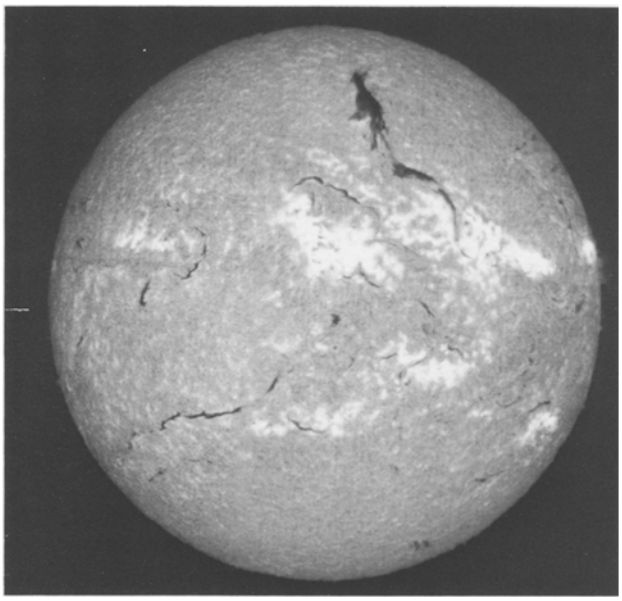

Fig. 6d.

TABLE II

Positions and temperatures of the LTR observed at 22 and 37 GHz

Date	UT_{22}	ϕ_{22}	CMD_{22}	ΔT_{22}	UT_{37}	ϕ_{37}	CMD_{37}	ΔT_{37}
14	13:50	53°	−35°	−720	–	–	–	–
15	07:11	55°	−25°	−630	09:13	52°	−23°	−900
16	07:07	54°	−5°	−550	07:45	56°	−10°	−860
17	07:44	55°	+9°	−590	08:18	53°	+4°	−860
18	07:49	48°	+19°	−320	08:20	49°	+17°	−470

TABLE III

Heliographic coordinates of the 'July 1982 filament'

Date	UT	ϕ_f	CMD_f	CMD_{fp}
14	10:23	50°	−40°	−30°
15	13:23	52°	−25°	−20°
16	13:35	56°	−10°	+1°
17	06:54	53°	+3°	+5°
18	08:39	49°	+16°	+9°

6. Large-Scale Patterns – Giant Cells

The superpositions of LTR locations in the synoptic maps reveal elliptical and circular patterns giving the impression of giant cell-like structures, similar to the patterns found by Schröter and Wöhl (1976), Schröter *et al.* (1978), Schwan and Wöhl (1978), Bumba (1987), Ambrož (1987). The superpositions of LTRs for three periods, well covered by observations are presented in Figure 7. In all maps one can identify several cells

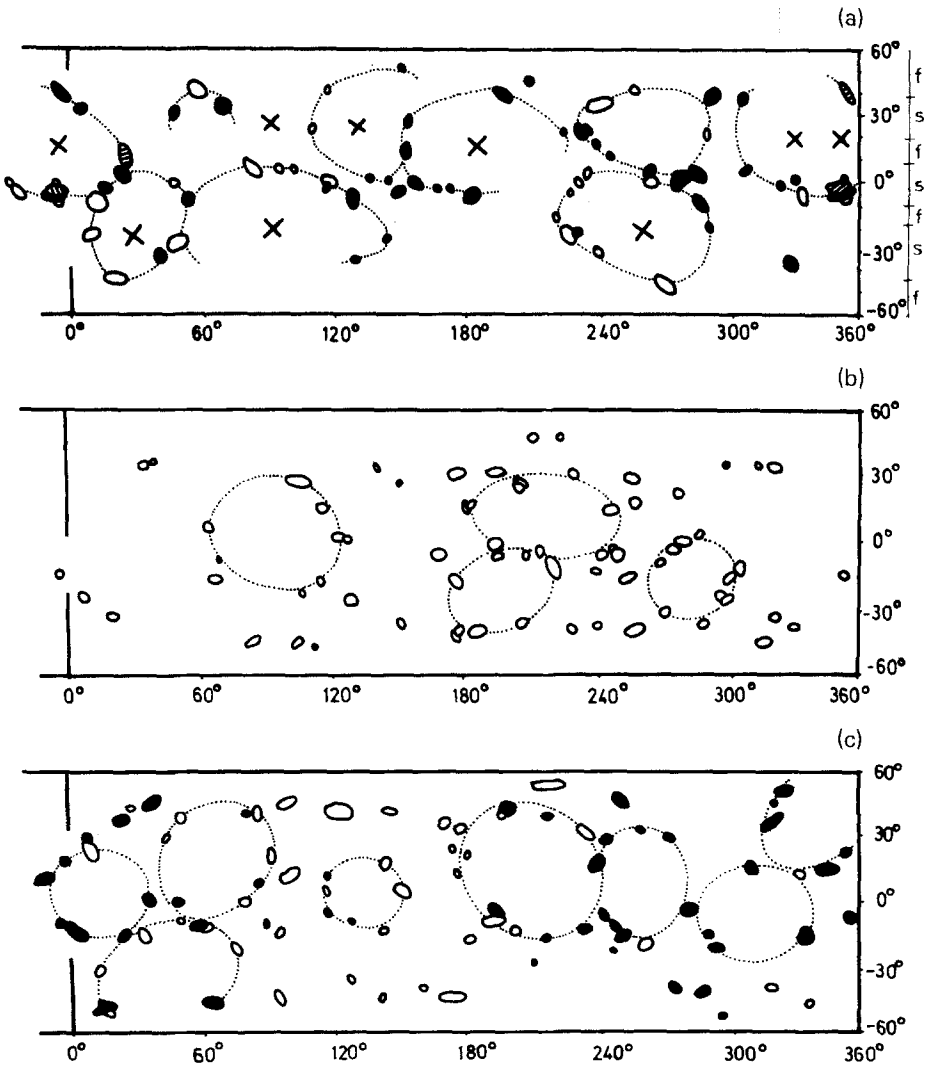

Fig. 7. (a) Superposition of the LTR positions in the period May 1979–May 1980 (black – May/June 1979; shaded – October 1979; white – May/June 1980). With dotted lines we outline the shapes of the 'giant cells' indicated by the distribution of LTRs. Crosses represent the positions of the centers of the 'giant cells' inferred by Bumba (1987) from magnetographic data. The belts of slow and fast rotation, as presented by Howard and LaBonte (1980) are denoted by the letters *s* and *f*, respectively. (b) Superposition of LTR positions in the period May–June 1981. (c) Superposition of LTR positions in the period May–August 1987 (black – May 1987; White – August 1987).

(indicated by the dashed line) consisting of 8–12 LTRs. A typical longitudinal extension of the features was 60° and the latitudinal dimensions were between 30° and 40°.

The map presented in Figure 7(a) is the superposition of the LTR positions obtained in the observational intervals May/June 1979, October 1979 and May/June 1980, i.e., it partly covers about a one-year time period (for details see Table I). The indicated cells embrace 87% of all LTRs in the map. Inspecting Figure 7(a) one finds that some cells persisted in only one observational subinterval. However, cells centered at coordinates $\lambda = 30°$, $\phi = -20°$; $\lambda = 90°$, $\phi = -20°$; $\lambda = 260°$, $\phi = +20°$; $\lambda = 260°$, $\phi = -20°$ and $\lambda = 300°$, $\phi = +20°$ were composed of LTRs appearing during the first as well as during the last observational interval (the observational subinterval in October 1979 was rather short so only the longitudes $\lambda = 300°–30°$ were covered). Such a long persistence of the large-scale patterns implies a rigid rotation of the elements constituting them (Stenflo, 1989). Pohjolainen *et al.* (1991) studied the properties of the LTR differential rotation obtained by tracing the LTRs day by day, and have found a really rigid rotation for the period 1979/1980. On the other hand, in the periods 1981/1982 and 1987 (related to the examples presented in Figures 7(b) and 7(c), covering the period May–June 1981 and May–August 1987, respectively) the LTRs behaved almost according to the 'standard' differential rotation law. So, the large-scale patterns appearing in these periods could not survive for more than few rotations in the most favorable cases when the patterns were close to the equator, which caused a rather intricate situation in the maps presented in Figures 7(b) and 7(c). The short life-time of the cell-like patterns was also inferred by Schröter and Wöhl (1976), Schröter *et al.* (1978), Schwan and Wöhl (1978), and Bumba (1987).

The period 1979/1980 overlaps with the study performed by Bumba (1987) who analyzed the global magnetic field patterns and also inferred possible cell-like structures. In the period embracing Carrington rotations No. 1681–1687 (April 1979–October 1980) he indicated (Plate 4 in Figure 5 therein) a number of possible cell-like structures. The magnetograms presented show rapid changes of the photospheric magnetic field patterns, however some cells were observed for several rotations. In Figure 7(a) we indicated by crosses the positions of the centres of Bumba's cells which could be identified during more than one rotation. Comparing the positions of Bumba's cells with the 'LTR-cells', one finds an intriguing correspondence. The cells centered at $\lambda = 180°$, $\phi = +15°$ and $\lambda = 90°$, $\phi = -20°$ were present in all of the magnetograms presented. The cell centred at $\lambda = 260°$, $\Phi = -20°$ can be identified on magnetograms covering rotations No. 1683–1686, while the other cells were seen only for two rotations. The LTR-cell between $\lambda = 300°$ and $\lambda = 20°$ at $\phi = +20°$ could be, in fact, related to two cells indicated in the magnetograms (lasting through rotations 1683–1684 and 1685–1686, respectively). The cell centred at $\lambda = 30°$, $\phi = -20°$ can be found only on the last magnetogram in the series (rotation No. 1687), but was notable in microwaves also in the May/June 1980 period.

In the period about the solar maximum, the cells were centred at heliographic latitudes about 20°. In Figure 8 we present the latitudinal distribution of LTRs simulated by taking 20° for the average heligraphic latitudes of the cell centred symmetrically with

respect to the equator, 60° and 40° for their longitudinal and latitudinal extension, respectively, and assuming a ring width of 10°. The effect of the visibility of LTRs (Figure 3(a)) was also included. Comparing the simulated distribution with the one

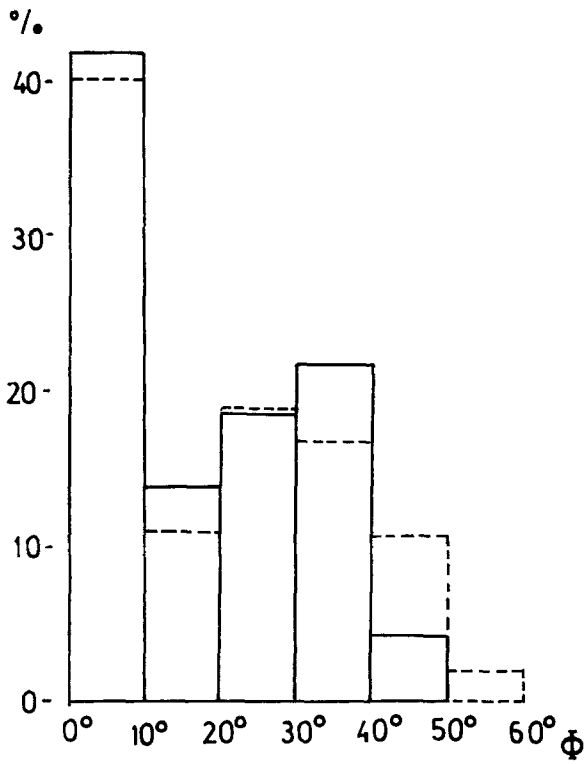

Fig. 8. Simulation of the latitudinal distribution of LTRs using the cell interpretation, corresponding to the period 1979/1980. The simulated distribution (full line) is obtained by taking into account the visibility of LTRs (Figure 3(a)) compared with the observed distribution (dashed line).

presented in Figure 3(b) one finds a good correspondence. Locations of the cell centres associated with the old cycle were distributed closer to the equator as the cycle proceeded to the minimum. In Figure 7(b) we present the synoptic map, with indicated cell-like structures, where we find several cells almost at the equator. Such a 'redistribution' of the cells during the cycle has caused the change of the latitudinal distribution shown in Figures 3(b) and 3(c). The cells associated with a new cycle appear at higher latitudes already at the maximum of the preceding cycle, as is shown by the butterfly diagram presented in Figure 4. In Figures 3(b) and 7(a) we have also indicated the positions of the zones of fast and slow rotation in the corresponding period as given in Howard and LaBonte (1980).

7. Discussion and Conclusion

The large sample of LTRs embraced in our study enables a reliable statistical analysis, and it shows that LTRs are directly associated with the inversion lines of the large-scale magnetic fields. An association with filaments is less obvious, since there are a considerable number of cases when LTRs were not associated with filaments, and also a large number of filaments did not produce observable LTRs. There are also discrepancies in the heights of the LTR perturbers inferred from the differential rotation study (Pohjolainen *et al.*, 1991). Still, one cannot exclude such an association, as one should expect strong absorption of the millimetric radiation in the dense plasma constituting the prominence (Chiuderi-Drago, 1990).

The appearance of a LTR without an associated filament could be explained by the presence of a coronal condensation which is too hot to appear as a prominence in the chromospheric lines, but still causing an absorption of millimetric waves (Kundu *et al.*, 1978). Using the coefficient for free-free absorption $k = 0.15N^2\nu^{-2}T^{-3/2}$ (Tucker, 1975) and a temperature $T = 20\,000$–$30\,000$ K and density $N = 5 \times 10^9$–10^{10} cm^{-3} one finds that the optical depth, $\tau = 1$, will be reached for a thickness of the order of 10^4 km. Similar conditions can appear after the thermal disparition brusques of quiescent prominences (Mouradian and Soru-Escaut, 1989). The appearance of a LTR in the absence of a filament could be caused also by a 'depression' in the transition region, associated with the magnetic inversion line. At the locations where the magnetic field is almost parallel with the temperature gradient (as should be expected at the inversion lines) the transition region is thinner than normal, and so it can be observed as a brightness temperature depression (Chiuderi and Chiuderi-Drago, 1991). On the other hand, an absence of LTRs in the presence of a filament can be explained simply by inadequate spatial resolution of the microwave observations and related temperature sensitivity: a small and weak 'source' will be smeared out and diluted, so the contrast might not be sufficient to be observed.

The evolution of the latitudinal distribution shows a similar behaviour as the one for the active regions, only appearing much earlier (already at the maximum of the preceding 11-year cycle). The LTRs are apparently grouped in two belts in the butterfly diagram, forming the borders of the active region belt and also showing an equatorward shift. This can be related to the equatorwards redistribution of the giant cells inferred from the superpositions of synoptic maps. Statistical considerations support the reliability of these cells, as well as does the consistency of the results with the ones from the independent study of magnetic field patterns presented by Bumba (1987). The typical longitudinal dimension of cells was about 60° which is consistent with some previous studies (Stix, 1989; Wöhl, 1990, and references therein). The lifetime of cells depended on the phase of the solar cycle. In the period 1979/1980 some cells could be identified during a period of one year, revealing a rigidly rotating component as depicted by Sheeley, Nash, and Wang (1987) and by Stenflo (1989). In other periods, the lifetimes were up to a few rotations, which is in accordance with the time variation of the LTR differential rotation law found by Pohjolainen *et al.* (1991).

Acknowledgements

We would like to thank Prof. J. O. Stenflo (ETH, Zürich) for helpful comments and discussions. R. Brajša would like to express thanks for the hospitality extended to him during his stay at Metsähovi Radio Research Station and acknowledges a grant from the Helsinki University of Technology.

The authors are very grateful to the referee, whose comments and suggestions have led to a substantial improvement of this paper.

Appendix

In order to check the reliability of the inferred giant cells described in Section 6, we performed a simple statistical analysis of the distribution of the cells on the synoptic map. We present an average cell as an elliptical ring. Taking for typical cell axes the values of 60° and 40°, respectively, and for the ring width 10°, one gets $A_0 = 2700$ deg^2 for the area outlined by the outer edge of the ring, and $A_v = 1200$ deg^2 for the area of the inner void, giving an estimate for the area of the ring $A_r = 1500$ deg^2. Furthermore we will take $A = 36000$ deg^2 for the area of the synoptic map between $\pm 50°$, where almost all LTRs appeared.

In order to simplify the problem, we will first consider the situation with only one cell on the map. We look for the probability that in the case of an accidental distribution (P_1) all of n LTRs constituting the sample ($n = 70$ in the situation presented in Figure 7(a)) fall out of the inner void, centred at the centre of one of Bumba's cells, and that x LTRs fall within the ring. One finds

$$P_1 = \binom{n}{x} (1 - p_v)^n p_r^x p_0^{n-x}, \tag{A1}$$

where

$$p_v = A_v/A, \tag{A2}$$

$$p_r = A_r/(A - A_v), \tag{A3}$$

and

$$p_0 = (A - A_0)/(A - A_v) \tag{A4}$$

are the probabilities that a LTR would fall in the void, would fall in the ring when the void is excluded, and would fall outside the ring when the void is excluded, respectively. The term $(1 - p_v)^n$ in Equation (A1) represents the probability that all LTRs fall outside the void. Taking into account Equations (A2)–(A4) one finds

$$P_1(x) = \binom{n}{x} (A_r/A)^x (1 - A_0/A)^{n-x}. \tag{A5}$$

In Figure 9 we present the functions $P_1(x)$ for different values of A_r/A and A_0/A in order to illustrate the probabilities for accidental appearance of the cells of different dimensions. For a typical cell, like the one centered at $\lambda = 255°$ and $\beta = -20°$ in Figure 7(a), which consisted of $x = 12$ LTRs, one finds, using

$$F_{x_0} = \sum_{x_0}^{n} P_1(x), \tag{A6}$$

that the probability of having $x \geq x_0 = 12$ LTRs in the ring is $F_{12} = 10^{-4}$ for a 'thick' cell (curve 3 in Figure 9) and $F_{12} = 10^{-6}$ for a 'thin cell' (curve 2 in Figure 9), which are

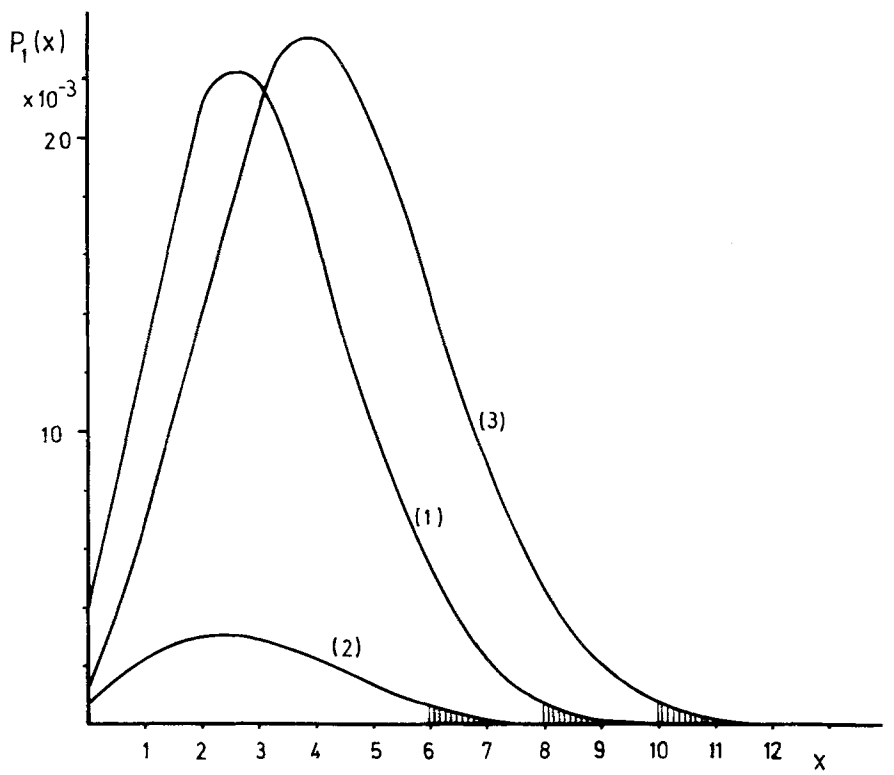

Fig. 9. Probability distributions for different cell sizes. Shaded areas represent the limit $F = 10^{-3}$. The curve 1 is obtained for a typical elliptical cell with axes of 60° and 40° and with a thickness of 10° ($A_0/A = 0.075$, $A_r/A = 0.042$). The curve 2 is obtained for a thinner and smaller cell ($A_0/A = 0.07$, $A_r/A = 0.04$). The curve 3 is obtained for a very large and very thick cell ($A_0/A = 0.09$, $A_r/A = 0.06$) representing an upper limit on cell dimensions.

both statistically entirely insignificant. The limit of $F = 10^{-3}$ is reached for 10 LTRs in the case of a large and thick cell (curve 3 in Figure 9). For other cases, this limit is shifted to a smaller number of LTRs (Figure 9). To clarify more directly these results, we performed a numerical experiment simulating an accidental distribution, and we found the same results as given by Equation (A5).

Taking into account that several cells are present simultaneously on the synoptic map (one finds at least 6 cells in Figure 7(a), embracing 87% of all LTRs in the map) the probability for accidental generation of cell-like patterns is reduced drastically.

To illustrate the reduction of the probability (when several cells are present) we consider a situation with only two distant cells. A similar procedure as used to obtain Equation (A5) gives

$$P_2(x_1, x_2) = \binom{n}{x}\binom{x}{x_1}(A_{r_1}/A)^{x_1}(A_{r_2}/A)^{x_2}(1 - (A_{01} + A_{02}/A))^{n-x}, \quad \text{(A7)}$$

where $x = x_1 + x_2$ and x_1 and x_2 are the numbers of LTRs in cell-rings of areas A_{r_1} and A_{r_2}, respectively. Approximating that the cells are equal, one finds

$$P_2(x_1, x_2) = \binom{n}{x}\binom{x}{x_1}(A_r/A)^{x}(1 - 2A_0/A)^{n-x}, \quad \text{(A8)}$$

which gives a much smaller probability for $x_1 \geq x_0$ and $x_2 \geq x_0$ than Equation (A6).

References

Ambrož, P.: 1987, *Bull. Astron. Inst. Czech.* **38**, 110.

Bumba, V.: 1987, *Bull. Astron. Inst. Czech.* **38**, 92.

Chiuderi-Drago, F.: 1990, in V. Ruždjak and E. Tandberg-Hanssen (eds.), 'Dynamics of Solar Prominences', *IAU Colloq.* **117**; *Lecture Notes in Physics*, Vol. 363, Springer-Verlag, Berlin, p. 70.

Chiuderi, C. and Chiuderi-Drago, F.: 1991, *Solar Phys.* **132**, 81.

Hiei, E., Ishiguro, M., Kosugi, T., and Shibasaki, K.: 1986, *Proc. Workshop on Coronal and Prominence Plasmas*, NASA Conf. Publ. 2442, p. 109.

Howard, R. and LaBonte, B. J.: 1980, *Astrophys. J.* **239**, L33.

Kundu, M. R., Fürst, E., Hirth, W., and Butz, M.: 1978, *Astron. Astrophys.* **62**, 431.

Liu, S.-Y. and Kundu, M. R.: 1976, *Solar Phys.* **46**, 15.

McIntosh, P. S.: 1972, in P. S. McIntosh and M. Dryer (eds.), *Solar Activity, Observations and Predictions*, MIT Press.

Mouradian, Z. and Soru-Escaut, I.: 1989, *Hvar Obs. Bull.* **13**, 379.

Pohjolainen, S., Vršnak, B., Teräsranta, H., Urpo, S., Brajša, R., Jurač, S., and Schroll, A.: 1991, in I. Tuominen, D. Moss, and G. Rüdiger (eds.), 'Sun and Cool Stars', *IAU Colloq.* **130**; *Lecture Notes in Physics*, Vol. 380, Springer-Verlag, Berlin, p. 279.

Schmahl, E. J., Bobrowsky, M., and Kundu, M. R.: 1981, *Solar Phys.* **71**, 311.

Schröter, E. H. and Wöhl, H.: 1976, *Solar Phys.* **49**, 19.

Schröter, E. H., Wöhl, H., Soltau, D., and Vazquez, M.: 1978, *Solar Phys.* **60**, 181.

Schwan, H. and Wöhl, H.: 1978, *Astron. Astrophys.* **70**, 297.

Sheeley, N. R., Jr., Nash, A. G., and Wang, Y.-M.: 1987, *Astrophys. J.* **319**, 481.

Stenflo, J. O.: 1989, *Astron. Astrophys. Rev.* **1**, 3.

Stix, M.: 1989, *The Sun*, Springer-Verlag, Berlin.

Tandberg-Hanssen, E.: 1977, in A. Bruzek, and C. J. Durrant (eds.), *Illustrated Glosary for Solar and Solar-Terrestrial Physics, Astrophys. Space Sci. Library*, Vol. 69, D. Reidel Publ. Co., Dordrecht, Holand, p. 102.

Tucker, W. H.: 1975, *Radiation Processes in Astrophysics*, MIT, Cambridge.

Urpo, S., Pohjolainen, S., and Teräsranta, H.: 1987, *Solar Microwave Radiation Maps Measured at Metsähovi Radio Research Station in 1978–79* (Report **A1**), Helsinki University of Technology.

Urpo, S., Pohjolainen, S., Teräsranta, H., Vršnak, B., Ruždjak, V., and Brajša, R.: 1989, *Hvar Obs. Bull.* **13**, 437.

Wöhl, H.: 1990, *Publ. Debrecen Heliophys. Obs.* **7**, 19.